BIOSCIENCES BIOTECHNOLOGY RESEARCH ASIA, October 2014. Vol. **11**(Spl. Edn. 1), p. 349-356

NiS/CdS Core-shell Embedded Polyaniline Composite: Synthesis and Characterization

T.R. Heera and V. Balasubramanian

Centre for ocean research, AMET University, Chennai - 603112, India.

doi: http://dx.doi.org/10.13005/bbra/1430

(Received: 15 August 2014; accepted: 10 October 2014)

The synthesis and characterization of the conducting polyaniline (Pani) films embedded with Co^{2+} doped, PVA capped NiS/CdS core-shell particles as photoluminescent boosters is reported. The photoluminescence intensity of the core-shell particles-Pani film had increased significantly. Periodic arrangement of the nanoclusters of the core-shell particles in the continuous conductive polymer matrix and high carrier density promise this material for the photoelectrochemical applications. Solid-state photovoltaic cells have been fabricated with NiS:Co/CdS-Pani as the electron conductor and Pani as the hole conductor. The cells show photocurrents of 0.1 mA/cm², voltages of 304 mV and energy efficiencies of 0.58%.

Key words: Composite materials; Polymers; Luminescence; Optical properties.

Considerable progress has been made in the preparation of metal sulfide semiconductor/ polymer composites due to their improved performance and potential applications. Composite materials made of conjugated polymer and metal sulphide quantum dots imparts unique opportunities for the fabrication of novel devices. The presence of conjugated Π electrons along the backbone of the polymers provides them the ability to support positive as well as negative charge carriers with high mobility along the chain. Interesting and unique physical properties are expected when the delocalised carriers interact with the semiconductor quantum dots. Potential areas of application of composite materials include nanoelectronics, low voltage flat panel displays, sensors, etc[1–5].

Pani is the most promising organic conducting polymer[6] for electronic applications due to its combination of electrical conductivity and environmental stability[7-9]. Various metal chalcogenide/polymer nanocomposites with desired functions have been prepared via an *in situ* reaction, such as II–VI sulfide/polymer nanocomposites[10, 11]. Compared to their individual constituents, the core-shell particles exhibit better physical and chemical properties thereby widening their applications range[12]. Significant efforts are devoted to fabricate core-shell colloidal sulphides with custom-specific structural, optical and surface properties[13, 14]. Among the various metal sulphides, nickel sulphide is one of the promising candidates[15-18]. As the size and extent of aggregation of the particles play a significant role in the optical properties, stabilization of the particles in suitable matrix is essential. The large surface to volume ratio in nanocomposites enables an efficient separation of photo-induced charges which is important for photovoltaic applications[19,20]. Efficient harnessing of solar energy through photoelectrochemical route is a promising option to meet the increasing energy demands. Conducting and luminescent boosters in such

* To whom all correspondence should be addressed.
E-mail: suresheera@gmail.com

systems will pave way for their enhanced efficiency. In this paper, we report a polymer-controlled growth strategy to prepare NiS/CdS core-shell particles embedded Pani composite films using polyvinyl alcohol (PVA) as the polymer-controller matrix by *in situ* method. The promising optical and electronic properties of the composites formed from these materials for the design of hybrid solar cells is reported.

EXPERIMENTAL

Polyvinyl alcohol (Kemphasol chemical Ltd), nickel chloride (Fischer Ltd), cobalt chloride (Fischer Ltd), cadmium acetate dihydrate (Fischer Ltd), aniline hydrochloride (Fischer Ltd) and ammonium persulphate (Fischer Ltd) were used for preparation without any further purification. All chemicals used were of AR grade. Hydrogen sulfide was prepared in laboratory using Kipp's apparatus. Double distilled water was used for the preparation of the solutions.

20 ml of 0.1 M of nickel chloride was added to 10% PVA solution followed by the addition of 20 ml of 0.25% cobalt chloride solution, H_2S gas and 11.5 ml of 2.5% of cadmium acetate dihydrate under constant stirring conditions. The colloidal solution obtained was sonicated for 5 minutes and then added to 25ml of aniline hydrochloride (0.2M) solution. 25 ml of ammonium persulphate (0.25M) solution was added under constant stirring conditions. The solution was stirred for 30 minutes to allow the polymerization to complete. From this solution free standing films of the core-shell composites embedded in Pani were formed by casting. The films were rinsed with dilute hydrochloric acid for the purpose of doping Pani. Pani film was washed with acetone to remove the oligomers. The film was dried at 80°C in an oven and used for further studies. The sequence of steps involved in the synthesis is given in flow chart (Fig.1).

RESULT AND DISCUSSION

UV Spectra

Fig. 2 shows the optical absorption spectra of NiS, NiS:Co, NiS:Co/CdS core-shell colloids along with that of Pani and Pani loaded with the core-shell colloids. An increase in absorbance is observed for the Co^{2+} doped NiS colloidal particles (Fig.2a, 2b). With the outer coverage CdS, the absorbance increases further (Fig.3c). For bulk NiS, CoS and CdS, the absorption edges are at 350 nm [21], 347 nm [21] and 515 nm [22] respectively. Blue shift in the absorption edge for NiS (280nm, Fig.3a) and NiS:Co (255nm, Fig.3b), from the corresponding bulk values, implies the quantum confinement effect of the nanoscale particles[23]. No other exciton peak or another steep edge in the UV region of the optical absorption spectra was observed indicating the absence of isolated CdS nanoparticles[24]. The absorption spectra of NiS in Pani (Fig.2d), NiS:Co in Pani (Fig.2e) and NiS:Co/CdS in Pani (Fig.2f) are shown in Fig.2. The Pani-colloid composite shows a wide absorption spectrum (Fig.2f) in the UV-Visible and near IR regions, suitable for harvesting of solar energy. The absorption spectrum of Pani is also shown for comparison (Fig.2g). The role of NiS:Co/CdS core-shell in increasing in the absorption intensity of Pani is evident from Fig.2f. In the

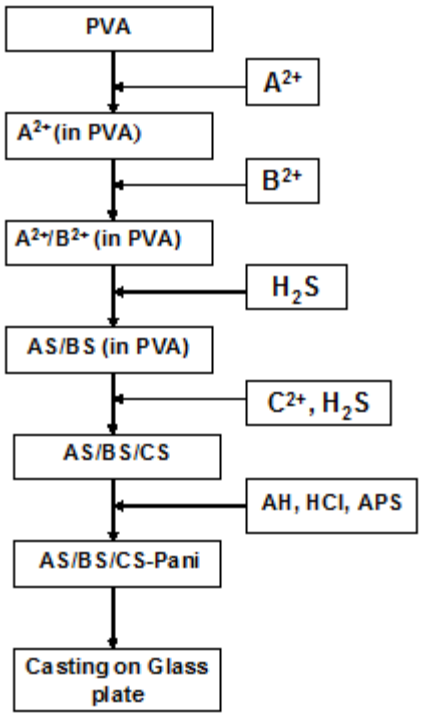

Fig. 1. Schematic diagram for the synthesis of NiS:Co/CdS-Pani composite. (Ni^{2+} core metal ion, Co^{2+}- dopant ion, Cd^{2+}-shell ion, AH-Aniline hydrochloride and APS-Ammonium persulphate)

absorption spectrum of Pani, the peak at 328nm is due to the π–π* transition within the benzenoid segment. The second shoulder-like absorption band at 450 nm is attributed to the doping level of Pani and the third absorption peak around 800 nm is related to the formation of localized polaron at the backbone of the polymer. The observed three characteristic peaks in absorption spectra indicate only pure emeraldine salt (ES) formed in the system without the formation of emeraldine base (EB) or leucoemeraldine base (LB) of Pani. The absorption peaks in core-shell composite embedded in Pani are due to the synergetic effects of polyaniline and the core-shell materials. The core-shell composite embedded in Pani shows a wide absorption spectrum in the UV-Visible and near infrared regions, much favourable for the photoelectrochemical harvesting of solar energy. Band gap energy and transition type was derived from mathematical treatment of the data obtained from the optical absorbance versus wavelength data with the following relationship for near-edge absorption:

$$\alpha = \frac{[k(h\nu - E_g)^{n/2}]}{h\nu} \quad ...(1)$$

where, α is absorption coefficient (cm^{-1}), h is the Plank's constant; ½ is the frequency of radiation (Hz), E_g is the energy band gap (eV) for

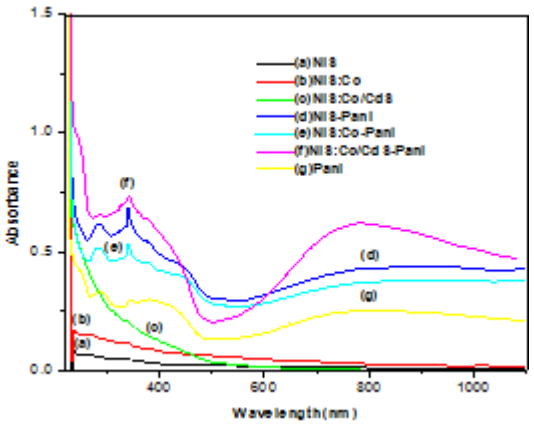

Fig. 2. UV-Visible absorption spectra of (a) NiS (b) NiS:Co (c) NiS:Co/CdS (d) NiS-Pani (e) NiS:Co-Pani (f) NiS:Co/CdS-Pani (g) Pani

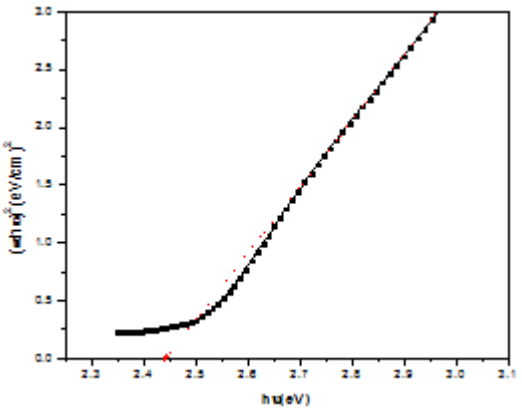

Fig. 3. Tauc plot for NiS:Co/CdS-Pani

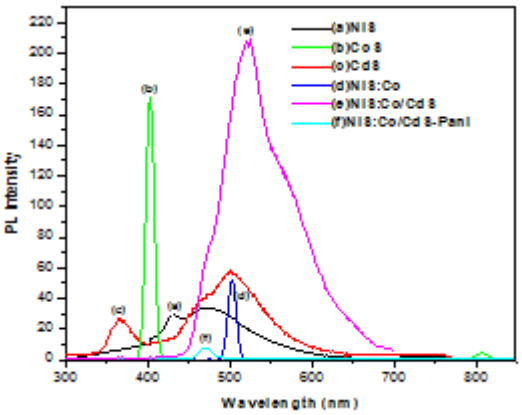

Fig. 4. Photoluminescence emission spectra of (a) NiS (b) CoS (c) CdS (d) NiS:Co (e) NiS:Co/CdS (f) NiS:Co/CdS-Pani

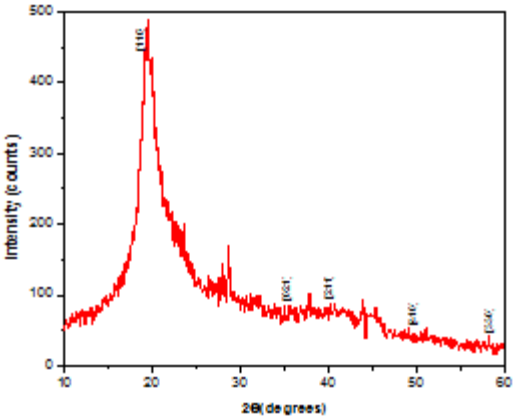

Fig. 5. XRD pattern of NiS:Co/CdS core-shell embedded Pani film

direct band gap semiconductor, k equals a constant while n carries the value of either 1 or 4. The bandgap, E_g, could be obtained from a straight line plot of $(\alpha h½)^{2/n}$ as a function of hÅ. Extrapolation of the line to the base line, where the value of $(\alpha h½)^{2/n}$ is zero, will give E_g [25]. If a straight line graph is obtained for n = 1, it indicates a direct electron transition between the states of the semiconductor, whereas the transition is indirect if a straight line graph is obtained for n = 4. Fig. 3 shows the Tauc plot for NiS:Co/CdS-Pani system. Extrapolation of the straight line portion of the graph to $\alpha = 0$ gives a band gap energy of 2.43 eV for NiS:Co/CdS-Pani. The straight line behaviour infers the direct transition between the states of the semiconductor composite.

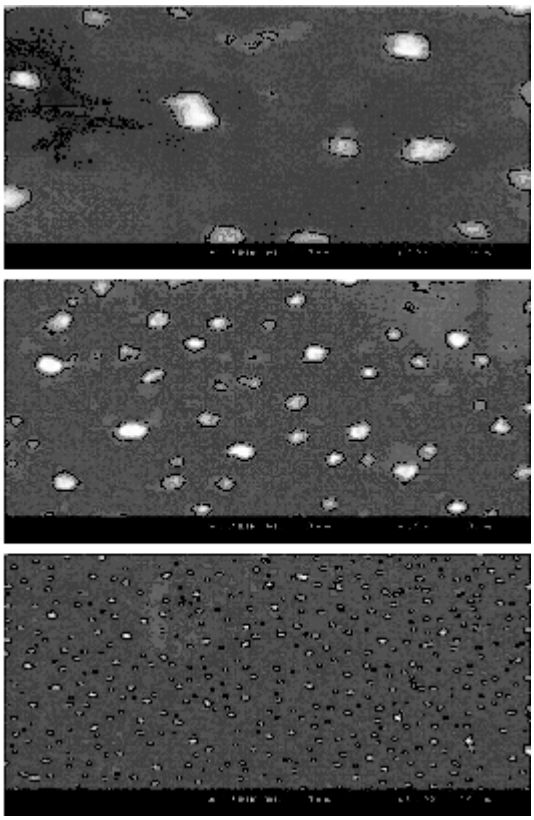

Fig. 6. Scanning Electron Micrograph of NiS:Co/CdS core-shell particles embedded Pani film, at three different magnifications

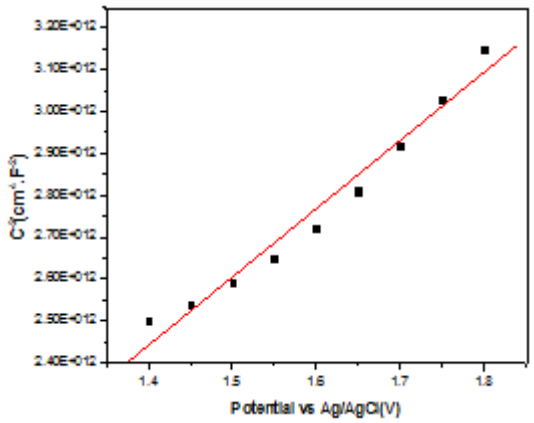

Fig. 7. Mott schottky plot of NiS:Co/CdS core-shell particles embedded Pani film

Photoluminescence

The PL spectra for NiS, CoS, CdS, NiS:Co, NiS:Co/CdS core-shell particles and NiS:Co/CdS-Pani are shown in Fig.4 at an excitation wavelength of 300 nm. The PL spectrum of NiS (Fig.4a) shows the blue band at 431 nm (2.87 eV) due to the band-edge emission, with about 1.07 eV blue shift compared to the bulk crystal (1.8 eV) [26] due to the quantum size effect. The PL spectra for CoS (Fig.4b) shows the near band edge intense emission at 404 nm and a weak emission at 808 nm while NiS:Co (Fig.4d) exhibits sharp emission peak at 500 nm. The PL spectrum of CdS (Fig.4c) shows peaks at 365 nm and 501 nm. The PL spectrum of NiS:Co/CdS (Fig.4e) exhibits strong and broad peak centered at about 523 nm with increased photoluminescence emission. For the physically mixed system of NiS and CdS, the PL intensity would register a decrease at their characteristic emission peaks whereas for the core-shell formation the PL intensity increases[27]. While the doping of NiS with Co^{2+} had red shifted the PL peak, shell formation with CdS has enormously increased the emission intensity over the visible range and hence acts as the booster for the incident visible light much preferred for the photoelectrochemical systems. The suppression of the PL emission peak of CdS at 386 nm and a hyperchromic effect at 520 nm highlights the surface passivation of the shell of CdS. The red shift in the PL peak is attributed to the partial leakage of exciton into the CdS layer and its confinement to the shell. Addition of Pani suppresses the photoluminescence (Fig.4f). The decrease in the PL intensity values at all wavelengths is due to fact that Pani is non-fluorescent and it disallows the recombination of photogenerated charges.

XRD studies

X-ray powder diffraction (XRD) analysis was carried out to investigate the phase of the NiS:Co/CdS-Pani composite. A typical XRD pattern of the film is shown in Fig.5. Particle size of about 96 nm was evaluated by Scherrer equation. Peaks have been indexed and suggest that the core material formed was NiS with rhombohedral crystal structure with cell parameters *a* = 9.620 Å and c = 3.149 Å, which are close to the data in JCPDS card no. 12-0041 and also reported by Qingtao Pan *et al*.,[26]. Separate peaks characteristic of CoS or CdS are not observed. The presence of a small foreign ion inclusion [28] or a shell layer over the core does not affect the XRD peaks of the core particles[29, 30].

SEM Analysis

Scanning electron microscopy is a convenient technique to study the microstructure of thin films. Fig. 6 shows the scanning electron microscopic image of the NiS:Co/CdS-Pani film at three different magnifications. The uniform distribution of the core-shell particles is well evident. SEM provides evidence for the stabilization of the core-shell particles-Pani composite by its periodic arrangement. Nanoscale aggregation of the particles is also observed from SEM images. From the SEM images it is observed that the NiS:Co/CdS-Pani composite has near spherical particles of about 300 nm. Higher resolution SEM images could not be obtained as the polymeric matrix developed charging and charing.

Mott-Schottky plot

The Mott-Schottky plot was constructed of the inverse square of space charge layer capacitance measured at a fixed frequency of 10000 Hz as a function of potential[31, 32]. The paramagnetic characteristic of this composite material was also confirmed by the magnetic susceptibility measurement using Sherwood Auto MSB meter. The Mott-Schottky plot (Fig.7) shows a positive slope for the, NiS:Co/CdS core-shell particles embedded Pani film indicating a typical n-type of the semiconductor. The flat-band potential, E_{fb}, is inferred from the intersection of the plot with the x-axis, as E_{fb}=1.37 V. The carrier density is evaluated as $8.65x10^{17}$.

AC Impedance

Features in the impedance spectra of electrochemical systems are related to physicochemical processes, occurring in the system when electric current passes through it [21] J.R. Macdonald, Impedance Spectroscopy : Emphasizing Solid Materials and Systems, Wiley, New York (1987)[33, 34]. Charge transfer resistance (R_{ct}) is a characteristic quantity for an electrode reaction indicative of electron transfer kinetics.

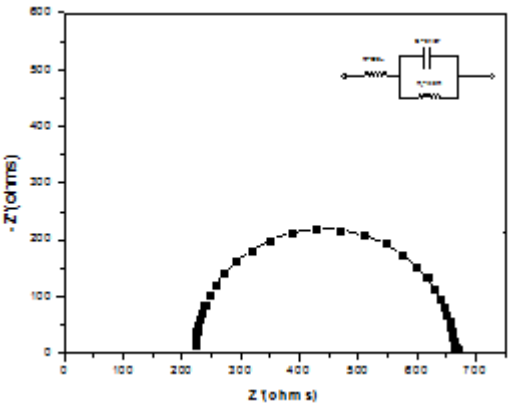

Fig. 8. AC Impedance spectra of NiS:Co/CdS core-shell particles embedded Pani film (inset equivalent circuit)

a) b)

Fig. 9. Photographs of (a) NiS:Co/CdS particles in PVA matrix (b) NiS:Co/CdS core-shell particles embedded in Pani matrix

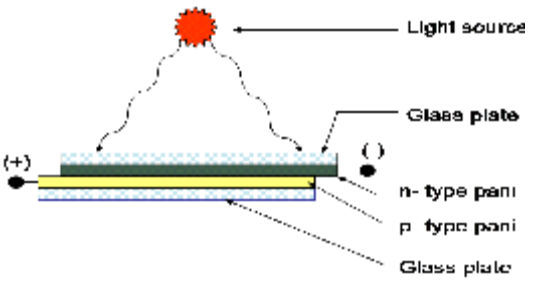

Fig. 10. Schematic diagram of soild state solar cell assembled

Thus a large charge-transfer resistance indicates a slow reaction. The curvature of the *Nyquist plot* in Fig.8 at high frequencies represents the *double-layer capacitance* in parallel with the charge transfer resistance. From the AC impedance spectrum (Fig.8), the charge transfer resistance of the film was found to be 440 ©. The equivalent circuit for NiS:Co/CdS-Pani film is also shown which reveals a double layer capacitance of 0.1µF. In such cases of low capacitance the equivalent circuit is simply modeled with the two resistances in parallel.

Conductivity Measurement

Fig.9 shows the NiS:Co/CdS core-shell particles in PVA matrix (a) and NiS:Co/CdS core-shell particles in Pani matrix (b). The conductivity of the core-shell particles embedded Pani film was 0.03 S/cm as evaluated by the four probe method.

I-V characteristics

A photoelectrochemical cell with an active area of 2 cm^2 was fabricated with NiS:Co/CdS-Pani film (n-type) as the anode and pristine pani film (p-type) as the cathode. Pani has been successfully used as a hole conductor material to fabricate the solid-state solar cells[35-40]. Fig. 10 shows the schematic diagram of solid state solar cell assembled. The current voltage characteristics of the cell was evaluated (Fig.11) with a white light source of intensity 15 mW/cm^2. P_{max} was found to be 0.088mW/cm^2 while the V_{oc} and I_{sc} are 304 mV and 0.1 mA/cm^2 respectively. The calculated cell efficiency and fill factor are 0.58% and 0.29 respectively.

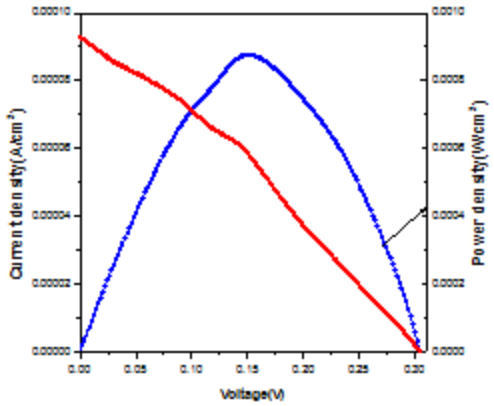

Fig. 11. Solar cell performance of solid state solar cell assembled with NiS:Co/CdS-Pani (n-type) and pristine Pani (p-type)

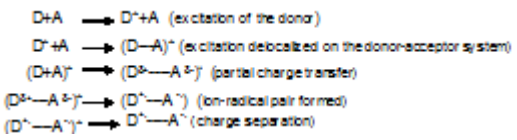

Fig. 12. Mechanism for photoinduced charge separation in a hybrid film under visible light

Mechanism

When photoexcited, Pani acts as electron donor. The excitated electron will be transferred from photoexcited Pani to the core-shell particle. The mechanism (Fig.12) below displays the photoinduced charge separation in a hybrid film of conducting polymer and high electron affinity core-shell particles[41, 42]:

CONCLUSION

Room-temperature synthesis of n-type semiconductors materials based on core-shell structures in Pani matrix has been optimized and reported. The UV-Visible absorption and emission spectra of NiS:Co/CdS-Pani revealed the step-wise spectral modifications effected by the preparation method. The scanning electron micrographs revealed core-shell structure and their periodic arrangement in the polymer matrix. The conductivity and carrier density promise this material for the photoelectrochemical applications. Solid state solar cell has been fabricated and evaluated. This configuration, with no liquid electrolyte, is easy for scale-up and effective for installation at any angle to harness maximum solar radiation.

REFERENCES

1. Qinqin Zhou, Yingru Li, Liang Huang, Chun Li and Gaoquan Shi Three-dimensional porous graphene/polyaniline composites for high-rate electrochemical capacitors *J. Mater. Chem. A*, 2014; **2**:17489.
2. Li Wang, Xingping Lu, Shengbin Lei , Yonghai Song," Graphene-based polyaniline nanocomposites: preparation, properties and applications" *J. Mater. Chem. A*, 2014; 4491-4509
3. Susmitha Uppugalla, Umashankar Male and Palaniappan Srinivasan "Design and synthesis of heteroatoms doped carbon/polyaniline hybrid material for high performance electrode in supercapacitor application" *Electrochimica Acta*, 2014; **146**: 242.

4. Xingping Lu, Yinjian Ye, Yingzhen Xie, Yonghai Song, Shouhui Chen, Ping Li, Lili Chen and Li Wang "Copper coralloid granule/polyaniline/ reduced graphene oxide nanocomposites for nonenzymatic glucose detection" *Anal. Methods*, 2014; **6:** 4643.
5. Hongyu Mi, Jiapan Zhou, Qingxia Cui, Zongbin Zhao, Chang Yu, Xuzhen Wang and Jieshan Qiu "Chemically patterned polyaniline arrays located on pyrolytic graphene for supercapacitors" *Carbon*, 2014; **80**: 799.
6. Yunyun Yang, Yanfei Hao, Junhua Yuan Li Niu, Fang Xia " In situ preparation of caterpillar-like polyaniline/carbon nanotube hybrids with core shell structure for high performance supercapacitors" *Carbon Volume* 2014; **78**: 279–287.
7. Guerfi, J. Trottier, I. Boyano, I. De Meatza, J.A. Blazquez, S. Brewer, K.S. Ryder, A. Vijh, K. Zaghib "High cycling stability of zinc-anode/ conducting polymer rechargeable battery with non-aqueous electrolyte" *Journal of Power Sources* 2014; **248**(15): 1 099–1104.
8. Xiaoning Tang, Mingwei Tian, Lijun Qu, Shifeng Zhu, Xiaoqing Guo,Guangting Han,Kaikai Sun,Xili Hu,Yujiao Wang,Xiaoqi Xu "A facile fabrication of multifunctional knit polyester fabric based on chitosan and polyaniline polymer nanocomposite" *Applied Surface Science* 2014; **317**: 505–510
9. D.Y. Liu , G.X. Sui, D. Bhattacharyya Synthesis and characterisation of nanocellulose-based polyaniline conducting films Composites *Science and Technology*, 2014; **99**: 31–3
10. Thomas Rath, Gregor Trimmel," In situ syntheses of semiconducting nanoparticles in conjugated polymer matrices and their application in photovoltaics "Hybrid Materials. Volume 1, Issue 1, ISSN (Online) 2299-3940
11. Yueqin Shi, Licheng Tan, Lie Chen Yiwang Chen, ", In Situ Fabricating One-Dimensional Donor–Acceptor Core–Shell Hybrid Nanobeams Network Driven by Self-Assembly of Diblock Copolythiophenes *Macromolecules* 2014; **47**(5): 1757–1767.
12. Xinhui Xia, Dongliang Chao, Zhanxi Fan, Cao Guan, Xiehong Cao, Hua Zhang, and Hong Jin Fan, " A New Type of Porous Graphite Foams and Their Integrated Composites with Oxide/ Polymer Core/Shell Nanowires for Supercapacitors: Structural Design, Fabrication, and Full Supercapacitor Demonstrations" *Nano Lett.*, 2014; **14**(3): 1651-1658.
13. Kevin J. Whitcomb , Jessica Q. Geisenhoff ,Duncan P. Ryan , Martin P. Gelfand , and Alan Van Orden , "Photon Antibunching in Small Clusters of CdSe/ZnS Core/Shell Quantum Dots" *J. Phys. Chem. B, Article ASAP* DOI: 10.1021/jp5083856 Publication Date (Web): September 18, 2014
14. Young-Shin Park , Wan Ki Bae , Lazaro A. Padilha ,Jeffrey M. Pietryga , and Victor I. Klimov * Effect of the Core/Shell Interface on Auger Recombination Evaluated by Single-Quantum-Dot Spectroscopy *Nano Lett.*, 2014; **14**(2): 396-402.
15. Jiaqin Yang, Wei Guo, Di Li, Caiying Wei, Hongmin Fan, Liyan Wu, Wenjun Zheng "Synthesis and electrochemical performances of novel hierarchical flower-like nickel sulfide with tunable number of composed nanoplates" *Journal of Power Sources*, 2014; **268**: 113–120
16. Wei Chen , Chuan Xia , and Husam N. Alshareef *One-Step Electrodeposited Nickel Cobalt Sulfide Nanosheet Arrays for High-Performance Asymmetric Supercapacitors *ACS Nano*, 2014; **8**(9): 9531–9541
17. Yanhong Li, Liujun Cao, Lei Qiao, Ming Zhou, Yang Yang, Peng Xiao, Yunhuai Zhang," Ni–Co sulfide nanowires on nickel foam with ultrahigh capacitance for asymmetric supercapacitors" *J. Mater. Chem. A*, 2014; **2:** 6540-6548
18. S. Nagaveena, C.K. Mahadevan," Preparation by a facile method and characterization of amorphous and crystalline nickel sulfide nanophases" *Journal of Alloys and Compounds* 2014; **582**: 447-456 .
19. Jun Yang, Jing-Jing Zhao, Chun-Rui Han, Jiu-Fang Duan, Feng Xu, Run-Cang Sun, "Tough nanocomposite hydrogels from cellulose nanocrystals/poly(acrylamide) clusters: influence of the charge density, aspect ratio and surface coating with PEG" *Cellulose February* 2014; **21**(1): 541-551
20. R. Mincheva, Ph. Leclère, Y. Habibi, J.-M. Raquez, P. Dubois, " Preparation of narrowly dispersed stereocomplex nanocrystals: a step towards all-poly(lactic acid) nanocomposites" *J. Mater. Chem. A*, 2014; **2**: 7402-7409
21. Sh.Sohrabnezhad, A. Pourahm d, Nickle oba t sulfide nanoparticles grown AlMC-41 type zolit, Physica E, **40**(28)6..
22. S. S. Kawar, B. H. Pawar, "Synthesis and characterization of cds n-type of semiconductor thin films having nanometer grain size" *Chalcogenide Lett.* 2009; **6** : 219.
23. A.Z. Malik, P.O. 'Brien, N. Revaprasadu, "Molecular design and development of single-component molecular metals" *J. Mater. Chem* 2001; **11**: 2382.

24. B. Saraswathi Ammaa, K. Manzoorb, K. Ramakrishnaa, M. Pattabi, "Synthesis and optical properties of CdS/ZnS coreshell nanoparticles", *Mater Chem Phys.* 2008; **112**: 789.

A. Kassim, T.W. Tee, A.M. Sharif, D.Y. Abdullah, M.J. Haron, H.S. Min, N. Saravanan, "Influence of bath temperature and pH value on properties of chemically deposited Cu4SnS4 thin films" *J. Chil. Chem. Soc.* 2009; **54**: 256.

25. Q. Pan, K. Huang, S. Ni, F. Yang, D. He, *Mater Res Bull.* 2008; **43**: 1440.

26. S.Y.Lu, M.L. Wu, H.L. *Chen, J. Appl. Phys.* 2003; **93**: 5789.

27. A.R. Kortan, R. Hull, R.L. Opila, M. G. Bawendi, M.L. Steigerwald, P.J Carroll L.E. Brus, *J. Am. Chem. Soc.* 1990; **112**: 1327.

28. H.Yang, P.H. Holloway, G. Cunnigham, K.S. Schanze , "CdS: Mn nanocrystals passivated by ZnS: synthesis and luminescent properties" *J. Chem. Phys.* 2004; **121**: 10233.

29. Ali 0mran Vaizoullar, Ahmet Balc1 Synthesis and Characterization of ZnO/SiO2 Core-Shell Microparticles and Photolytic Studies in Methylene Blue Int. *J. Res. Chem. Environ.* 2014; **4**(2): 161-165.

30. Andac Arslan a, Evrim Hur a, Saliha Ilican b, Yasemin Caglar b, Mujdat Caglar Controlled growth of c-axis oriented ZnO nanorod array films by electrodeposition method and characterization Spectrochimica Acta Part A: *Molecular and Biomolecular Spectroscopy* 2014; **128**: 716–723

31. K.Geldermann, L. Lee, S.W. Donne, Flat-band potential of a semiconductor: using the Mott–Schottky equation *J. of Chem Educ.* 2007; **84**: 685.

32. A.J.Bard, L.R. Faulkner, Electrochemical Methods: Fundamentals and Applications, Wiley, New York 1980.

33. J.R. Macdonald, Impedance Spectroscopy: Emphasizing solid Materials and systems, Wiley, New York 2000.

34. Z. Liu, J. Zhou, H. Xue, L. Shen, H. Zang , W. Chen , Polyaniline/TiO_2 solar cells Synthetic Met. 2006; **156**: 721.

35. Neelam Saurakhiya , Satinder K. Sharma, Rudra Kumar ,Ashutosh Sharma "Templated Electrochemical Synthesis of Polyaniline/ZnO Coaxial Nanowires with Enhanced Photoluminescence" *Ind. Eng. Chem. Res., Article ASAP Publication Date* (Web): 2014 .

36. Yaoming Xiao, Gaoyi Han, Yunzhen Chang, Haihan Zhou, Miaoyu Li, Yanping Li "An all-solid-state perovskite-sensitized solar cell based on the dual function polyaniline as the sensitizer and p-type hole-transporting material " *Journal of Power Sources* 2014; **267**: 1-8.

37. S. Tan, J. Zhai, B.Xue, M.Wan, Q. Meng, Y.Li, L. Jiang. D. Zhu, Photocurrent induced by conducting channels of hole transporting layer to adjacent photoactive perovskite sensitized TiO2 thin film: Solar cell paradigm Langmuir, DOI: 10.1021/la502398x Publication Date (Web): 2014.

38. Anurag Krishna, Dharani Sabba, Hairong Li, Jun Yin, Pablo P. Boix, Cesare Soci, Subodh G. Mhaisalkar and Andrew C. Grimsdale Novel hole transporting materials based on triptycene core for high efficiency mesoscopic perovskite solar cells *Chem. Sci.*, 2014; **5**: 2702-2709.

39. Zhang Xiaoping, Lan Zhang, Wu Jihuai, Lin Jianming, Fan Leqing "Enhancing photovoltaic performance of photoelectrochemical solar cells with nano-sized ultra thin Sb_2S_3-sensitized layers in photoactive electrodes" Journal of Materials Science: Materials in Electronics June 2013; **24**(6): 1970-1975.

40. N.S. Sariciftci, A.J. Heeger, Handbook of conductive molecules and polymers, John Wiley and Sons, New York, 1997.

41. J.Heeger, *Reviews of modern Physics.* 2001; **73**: 681.